

# Thermo-accelerative optimization of relativistic lightsails

John Brewer,<sup>†</sup> Matthew F. Campbell,<sup>‡</sup> Pawan Kumar,<sup>¶</sup> Sachin Kulkarni,<sup>†</sup> Deep  
Jariwala,<sup>¶</sup> Igor Bargatin,<sup>‡</sup> and Aaswath P. Raman<sup>\*,†</sup>

<sup>†</sup>*Department of Materials Science and Engineering, University of California, Los Angeles,  
Los Angeles, CA*

<sup>‡</sup>*Department of Mechanical Engineering and Applied Mechanics, University of  
Pennsylvania, Philadelphia, PA*

<sup>¶</sup>*Department of Electrical and Systems Engineering, University of Pennsylvania,  
Philadelphia, PA*

E-mail: aaswath@ucla.edu

## Abstract

The Breakthrough Starshot Initiative aims to send a gram-scale probe to Proxima Centuri B using a high-power laser-accelerated lightsail traveling at relativistic speeds. Thermal degradation is a key consideration in the design of lightsails because the intense laser power required will heat sails to extreme temperatures. Previous work has evaluated lightsails primarily based on their acceleration distance, with thermal considerations being a secondary concern. In this work, we demonstrate co-optimization of accelerative and thermal performance for sail designs that use a multilayer connected photonic crystal composed of layered 2H-phase Molybdenum Disulfide and crystalline Silicon Nitride. We highlight the inverse relationship between thermal band extinction coefficient and lightsail maximum steady state temperature, then characterize the

trade-off between acceleration distance and maximum sail temperature. Additionally, we introduce thermally durable acceleration minimum (TEAM) as a summary result that characterizes the best realistic acceleration distance achievable within a sail design space, and report a TEAM value of 16.2 Gm for our class of designs. We conclude by demonstrating a multiscale Mie resonance-based approach to enhancing sail emissivity over infrared wavelengths that simultaneously preserves favorable lightsail acceleration distance characteristics.

## Keywords

Starshot, lightsail, Photon Momentum, Infrared, Nanophotonics, Mie Resonance, Photonic Crystal Reflector, 2D Materials, Silicon Nitride, Molybdenum Disulfide

## 1 Introduction

Humanity’s exploration of interstellar space has long been considered to be a topic for science fiction, rather than contemporary scientific inquiry. While exploration within our solar system could be accomplished by many feasible propulsion schemes, the light year-scale distances involved in interstellar travel pose fundamental scientific and engineering challenges. Early nuclear pulse<sup>1</sup> and fusion power-based<sup>2-4</sup> methods were proposed but ultimately abandoned. More recently, the Breakthrough Starshot Initiative has proposed an ambitious and potentially feasible means of achieving interstellar travel within human lifetimes, by sending a small gram-scale probe 4.2 light years to Earth’s nearest habitable candidate exoplanet, Proxima Centauri B.<sup>5-7</sup> The proposed propulsion mechanism to traverse this immense distance is a laser-driven lightsail that is accelerated to one-fifth the speed of light, towing a probe-chip payload. Lightsails are highly reflective surfaces that are propelled using the concept of photon momentum transfer.<sup>8</sup> In the time since this phenomenon was first observed by Maxwell in 1873, lightsail-driven vehicles have been studied and theorized extensively for

solar,<sup>9–11</sup> astrophysical,<sup>12,13</sup> and laser<sup>14–17</sup> sources. JAXA’s IKAROS project has successfully explored the solar system using the low-intensity photon flux of our Sun.<sup>18</sup> In contrast, Starshot’s target velocity and destination require using a gigawatt-scale irradiance phased-array laser source, resulting in orders of magnitude greater light intensities on the sail and creating a unique and difficult problem in sail design and materials selection.

Realizing functional laser-driven sails necessitates solving a series of problems that lie at the intersection of material, mechanical, and optical engineering,<sup>19</sup> solutions to which have only recently been put within reach through advances in nanofabrication,<sup>20–22</sup> photonics,<sup>23–26</sup> and radiative cooling.<sup>27,28</sup> As the sail accelerates, incident laser light will become redshifted in the sail’s frame of reference. This sets a restriction on usable sail film materials to those that have little or no measurable absorption over the entire red-shifted laser band. The sail must furthermore be highly reflective over the laser band in order to accelerate to its ultimate speed quickly and limit the laser-on time. In addition to reflectivity, the sail must also exhibit sufficient mechanical robustness to survive the extreme acceleration-induced forces, as well as its interaction with the interstellar medium.<sup>29–31</sup> While accelerating, the sail must be shaped or patterned properly so as to stably ride the laser beam when faced with non-ideal beam shapes and alignments.<sup>32</sup> Finally, the sail must radiate any heat generated due to very weak absorption of sail materials, as there are no convective or conductive avenues for thermal regulation.

Motivated by the Breakthrough Starshot Initiative’s goals, pioneering work on this topic proposed and analyzed a range of lightsail designs that minimize laser requirements,<sup>19</sup> suggested the use of highly thermally emissive material layers for radiative cooling, examined how material laser band absorptivity can affect sail temperatures, and demonstrated a trade-off between sail reflectivity and mass through a newly defined figure of merit.<sup>33</sup> This was followed by demonstrations of methods to passively stabilize beam-riding surfaces using spherical, parabolic, and conical sail shapes.<sup>34</sup> Passive beam-riding stability of curved lightsails was then adopted to design and analyze flat metasurface and diffractive beam stable

structures and the opto-mechanical considerations of these sails, showing that their designs were able to meet a material melting point-based thermal sail limit.<sup>35,36</sup> Recent work has proposed designs that achieve even lower acceleration distances using generalized gradient descent and topological optimization methods for nanophotonic sail design.<sup>37</sup> While these works have demonstrated key advances in sail engineering, thus far they have only explored the use of Si, SiO<sub>2</sub>,<sup>33,35,36</sup> and Si<sub>3</sub>N<sub>4</sub><sup>37,38</sup> as sail materials. Additionally, the literature up to this point has not optimized designs for acceleration distance under thermal constraints, or determined how photonic designs might enhance emissivity over infrared wavelengths while also minimizing the sail mass and maximizing its reflection. More broadly, given an increasingly large range of sail designs and materials, it has become progressively more important to develop a methodology by which one can select and optimize sail designs constrained by their thermal performance and material degradation limits.

In this work we demonstrate and optimize a comprehensive nanophotonic sail design composed of MoS<sub>2</sub> and Si<sub>3</sub>N<sub>4</sub>. Additionally, we develop a thermal-accelerative co-optimization framework and accompanying metrics for sail designs to aid future designers in setting realistic acceleration distance goals that balance laser reflectance, thermal emissivity and the highest survivable operating temperature of the sail’s constituent materials. We analyze our class of sail designs using this framework and find a thermally durable acceleration minimum of 16.2 Gm for a 1g payload. Importantly, this sail design does not require additional layers for thermal emissivity purposes, with the payload mass including only probe mass and tethers. Finally, to improve thermal survivability further, we explore the use of a multiscale Mie resonator photonic reflector design that is able to provide emissivity gains and lower overall sail temperatures within an ultra-low mass budget. Our findings highlight the need for ultra-high sensitivity measurements of material absorption characteristics using techniques such as photothermal deflection spectroscopy<sup>39</sup> or photocurrent spectroscopy<sup>40,41</sup> in order to qualify lightsail materials, as well as the need for further research into the thermo-optic effects of candidate materials at temperatures ranging from 500 to 2000 K.

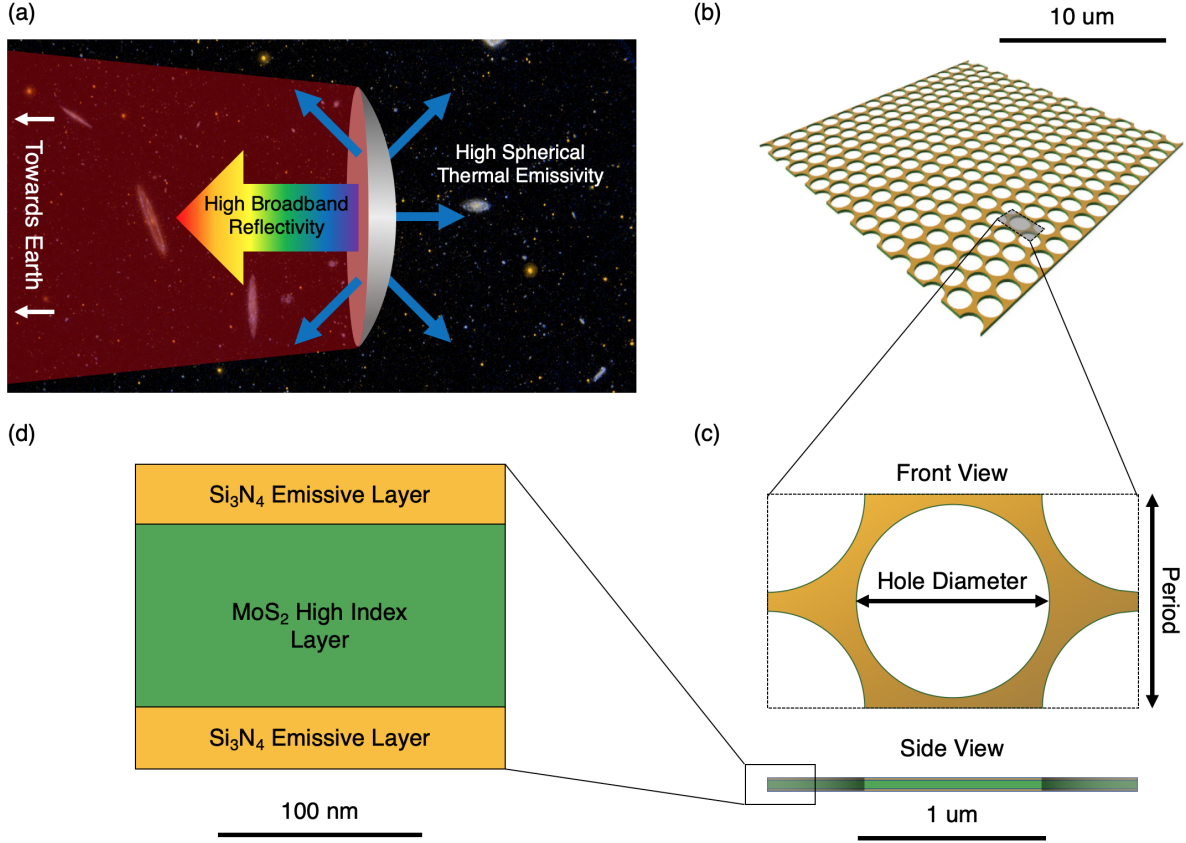


Figure 1: Starshot sail design. (a) Schematic diagram demonstrating relevant optical considerations for accelerating lightsail (b) Section of sail, approximate hole-fill ratio of 76% (c) Front and side view of single design period. (d) Enlarged view of multilayer structure. Yellow regions represent  $\text{Si}_3\text{N}_4$  while green regions represents  $\text{MoS}_2$ .

A relativistic laser-driven interstellar lightsail will encounter extreme conditions that place stringent requirements on its properties. The sail must have an ultra-low mass, be structurally robust, be highly reflective over a broad band corresponding to the laser wavelength and its red-shifted spectrum, and have sufficient thermal emissivity to radiatively cool, preventing material melting or sublimation. A central challenge in understanding the survivability of the sail lies in mapping the trade-off between the minimal absorption over laser wavelengths and emissivity at longer thermal wavelengths, given the need to maximize reflectivity in order to minimize acceleration distance for effective propulsion. Motivated by this challenge, we developed a multilayer 2D photonic crystal slab-based geometry that features  $\text{MoS}_2$  and  $\text{Si}_3\text{N}_4$  as its key constituent materials. Figure 1a illustrates the general

optical considerations of lightsail design, while Figures 1b and 1c show the hole diameter and period parameters we investigated in our periodic concept sails. Figure 1d details the thickness parameters of the layered structure of our design, which is composed of two emissive  $\text{Si}_3\text{N}_4$  outer layers surrounding a  $\text{MoS}_2$  high-index reflective core.

Previous work has discussed the possible use of  $\text{MoS}_2$  for laser-driven lightsails,<sup>19</sup> but its use in real sail designs is still unexplored. Here we choose to investigate designs employing  $\text{MoS}_2$  for three key reasons. The first is its high refractive index in the laser band, ranging from  $n = 3.73 - 3.66$ , which makes it a desirable reflective material. Second, monolayer  $\text{MoS}_2$  samples have been shown to have zero absorption in the expected laser bandwidth within measurement limits.<sup>42</sup> Finally, large area monolayer samples have been fabricated in the past, meaning future lightsail scale films may be possible.<sup>43–45</sup>

$\text{Si}_3\text{N}_4$  has also been recently investigated for lightsails<sup>37,38,46</sup> and remains a well-qualified lightsail candidate material due to its mature fabricability, low density, and high decomposition temperatures.<sup>47,48</sup> In addition to these considerations, our primary motivation for using this material is its desirable thermal emissivity at wavelengths longer than the Doppler-shifted laser band, which will be discussed in detail below.<sup>49</sup> As used in our sail design,  $\text{Si}_3\text{N}_4$  acts as the primary radiative cooler, preventing thermal failure during acceleration. We emphasize that in our design we do not assume the presence of an additional layer or layers that provide non-zero emissivity. Rather, the combined sail design is meant to be holistic and comprehensive.

Due to the stringent mass constraints of Starshot, the mass of this multilayer design is reduced, and laser reflectance enhanced, through the patterning of a 2D photonic crystal with a close-packed array of large-radius holes with respect to the lattice constant of the structure. Apart from mass considerations, the photonic design provides reflective enhancement through coupling to broadband guided modes, building on conventional 2D photonic crystal slab theory.<sup>24</sup> However, the extreme performance required of the lightsail requires designs typically not explored by conventional photonic crystal reflectors. Specifically, pre-

vious conventional photonic crystal reflector literature has not been mass constrained to our knowledge. Structurally, an important advantage of our proposed design is that it is fully connected and requires no additional substrate to function as a standalone sail.<sup>37</sup> In practice however, we expect it will be beneficial to use a large corrugated support backbone<sup>50</sup> to allow the sail to withstand the extreme forces it will undergo as it accelerates. This structure would provide macroscale sail curvature to increase stability and mechanical robustness<sup>51</sup> while additionally limiting crack propagation in our proposed designs due to patterned hole-induced stress concentrations.

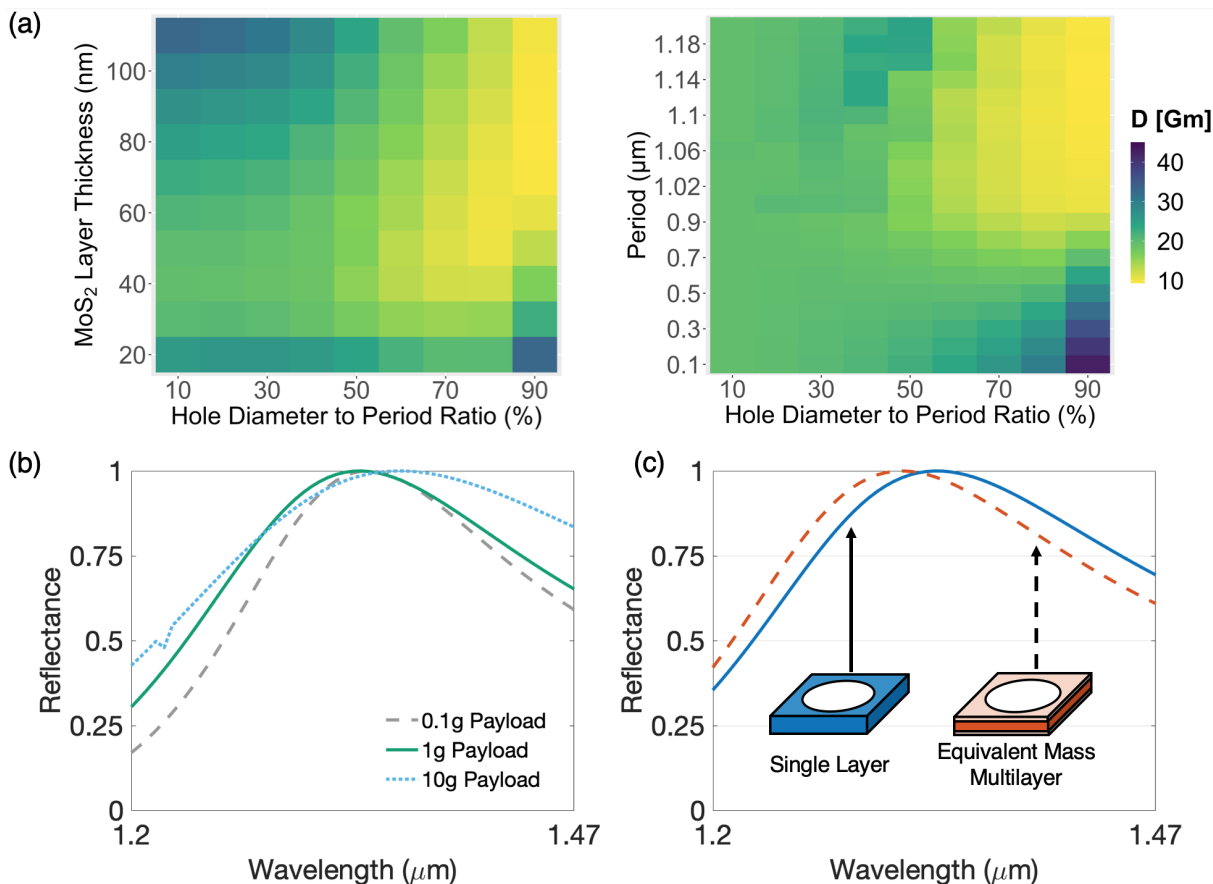


Figure 2: Reflective properties of multilayer photonic sail structures. (a) Color maps of minimum distance designs as a function of most sensitive geometric parameters. (b) Dependence of sail reflection spectra on payload mass. Lower mass payloads reward reduction in sail mass more than increase in integrated reflection spectra. (c) Demonstration of desirable spectral perturbation due to the addition of lower index, high emissivity Si<sub>3</sub>N<sub>4</sub> layers. Insets provide schematic diagrams of sail designs corresponding to plot colors

To optimize the sail design, we assumed typical values for the Starshot Initiative: a  $I = 10 \text{ GW}/m^2$  irradiance laser operating at  $\lambda = 1.2\mu\text{m}$ , a  $10 \text{ m}^2$  sail area, and a  $\sim 1 \text{ g}$  chip payload mass unless otherwise stated. The acceleration distance figure of merit, as defined by Jin et al.<sup>37</sup> is:

$$D = \frac{c^3}{2I} (\rho_{\text{payload}} + \rho_{\text{sail}}) \int_0^{0.2} \frac{h(\beta)}{R(\lambda(\beta))} d\beta$$

where  $h(\beta) = \frac{\beta}{(1-\beta)^2\sqrt{1-\beta^2}}$ ,  $I$  is the laser irradiance in  $\frac{W}{m^2}$ ,  $\rho$  is areal density in  $\frac{kg}{m^2}$ ,  $\beta$  is the unitless fractional speed of light, and  $R(\lambda(\beta))$  is the spectral reflectance over the Doppler-shifted laser band.

Optimizing period and hole diameter of the patterned holes allows for high transmission and reflection bands of varying spectral bandwidth.<sup>24</sup> Figures 2a and b demonstrate the dependence of acceleration distance on key design parameters in our sail design space. Each color map represents a two dimensional slice of the five dimensional design space composed of the period/lattice constant, the hole diameter-to-period ratio, and the thicknesses of each of the three layers. The tile colors represent the minimum acceleration distance design possible for the parameter values specified on the axis (this minimum is achieved by changing the unseen parameters to their optimal values for the given tile). Our optimal acceleration distance merited design has a period of  $1.14 \mu\text{m}$ , a hole diameter scale of 90%, 5nm thick emissive  $\text{Si}_3\text{N}_4$  layers, and an 80 nm thick  $\text{MoS}_2$  reflective core, placing it in a regime of very low values of thickness relative to lattice constant,  $< 0.1a$ . Thinning of the high-index core maintains access to broad-band Fabry-Perot-like reflection modes at normal incidence with the added effect of minimizing the overall sail mass. This demonstrates the broad range of possible acceleration distance values that our design space encompasses.

While the actual mass of the payload chip has not been determined yet, it is important to understand the relative effect of the payload mass on our optimal reflective design. Note that payload mass can be converted to the density value shown in the figure of merit easily by dividing its mass by sail area. Qualitatively, Figure 2c demonstrates that as the payload mass increases, sail mass is rewarded less than integrated reflectance, showing that sail

mass is a stronger consideration when the payload mass is low. A further analysis showing the minimum acceleration distance vs. payload mass can be found in the supplementary information, which is corroborated by results in Jin et al.<sup>37</sup>

The  $\text{Si}_3\text{N}_4$  layers have primarily been introduced to enhance thermal emissivity; however, these outer layers can also have the effect of shifting the peak of the sail reflection spectra to lower wavelengths compared to that of single-layer  $\text{MoS}_2$  designs, as shown in Figure 2c. This shift fortuitously results in an improvement in the acceleration distance figure of merit. Note that since the designs shown in Fig 2c have identical masses, this effect is attributable to the change in the refractive index profile alone.

The optimization procedure described thus far yields an optimal reflective design in this sample set of 9.8 Gm with a 1-g payload, comparable in performance to the best reported numbers in the literature.<sup>37</sup> However, unlike other designs, no supporting structure is required for this design type, and all sail mass necessary for propulsion is accounted for in this figure of merit value. Additional structural stability may be provided by a 1-g mechanical backbone structure, giving a value of 14.2 Gm. Furthermore, the topology of this design is not optimized, and optimization could yield still lower acceleration distances. While this design is competitive with others shown previously<sup>35,37</sup> on acceleration distance metrics alone, lightsails with realistic additional thermal considerations require 65% larger acceleration distances as we show in the following section.

Maintaining the sail's integrity as it accelerates is a fundamental consideration in design, more important than any acceleration distance or reflection-driven performance metric. Though the sail will exhibit extremely low absorbance, its temperature will nevertheless increase due to the high incident laser photon flux and interaction with the interstellar medium at relativistic speeds could cause even further heating.<sup>29</sup> Unfortunately, the sail's component materials will likely become more absorptive as their temperature rises, causing thermal runaway effects and increasing the probability of sail mechanical failure due to material degradation. With these considerations in mind, the radiative cooling characteristics

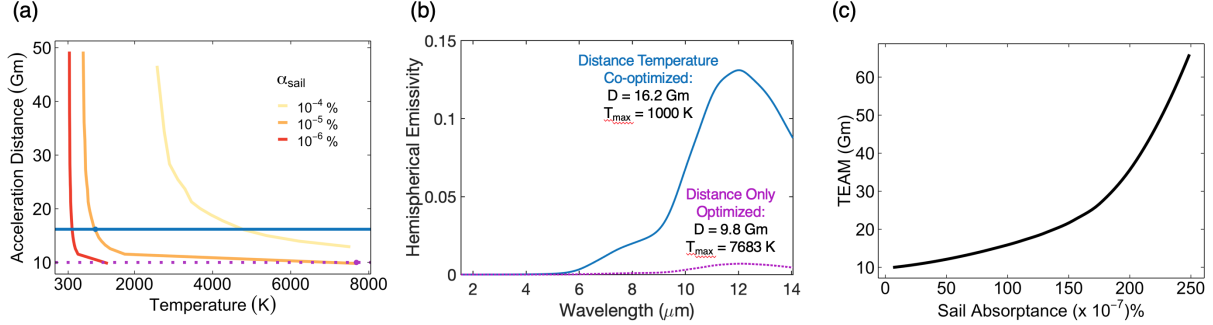


Figure 3: Emissive properties of multilayer photonic sail structures. (a) Minimum acceleration distance as a function of temperature for assumed values of sail absorptivity. Points and horizontal lines demonstrate how selected designs in (b) change temperature as assumed absorptivity is altered. (b) Emissivity comparison of acceleration-optimized design vs. acceleration temperature co-optimized design. Acceleration distance and maximum temperature of each design are also shown. (c) Plot showing our design space thermally endurance acceleration minimum (TEAM) value as a function of assumed lightsail absorptivity. TEAM is the thermally-constrained minimal acceleration distance design.

of the sail become extremely important. Recent sail design literature has cited the maximum allowable temperature of their designs as the melting temperature of their materials at atmospheric pressure. However, this is an unrealistically high temperature for the sail to reach in practice, because in the ultra high vacuum (UHV) of space the sail will begin to sublime before it melts. Due to this, we argue that either a material’s ultra-high vacuum vaporization temperature or decomposition temperature should be considered as its upper operational limit.

To proceed, our framework analyzes the maximum temperature reached by each design in our  $> 300,000$  design space. This is determined using the following equation:

$$P_{laser}\alpha_{sail} = 2A_{sail} \int_a^b \frac{c_1}{\lambda^5} \cdot \frac{\epsilon_{sail}(\lambda)}{e^{\frac{c_2}{\lambda T_{max}}} - 1} d\lambda$$

where  $P_{laser}$  is the output laser power (100 GW),  $\alpha$  is the assumed normalized sail absorption,  $A_{sail}$  is the sail emissive area,  $c_1 = 2\pi hc^2$ ,  $c_2 = hc/k_b$ , and  $\epsilon_{sail}$  is the spectral sail emissivity.

We determine the spectral hemispherical absorptivity of each design via a dimensionally-reduced simulation of sail designs, then assume the sail is always in thermal equilibrium

to equate absorptivity to emissivity using Kirchhoff’s law, and finally determine  $T_{\max}$  numerically. The motivation for the integral form shown can be found in the supplementary information. This approach allows us to estimate a high bound on  $T_{\max}$  for every investigated design. For the purposes of this work, we will use the thermal range from  $a = 1.55$  to  $b = 14.05$   $\mu\text{m}$ , the approximate data boundaries for  $\text{Si}_3\text{N}_4$  given in Kischkat et al.<sup>49</sup>  $\text{MoS}_2$  has not been investigated thoroughly in this band, and so we conservatively assume its emissivity in the thermal wavelengths to be 0. Further investigation of  $\text{MoS}_2$  could yield evidence of non-zero thermal band emissivity, leading to an overall reduction in maximum temperature values.

After determining the maximum temperature of each design, we then eliminate designs using the conservative UHV upper temperature limit applied to  $\text{MoS}_2$ . Based on previous thermodynamic analysis, the decomposition of  $\text{MoS}_2$  to  $\text{Mo}_2\text{S}_3$  occurs at  $\sim 1250$  K for a pressure of  $10^{-4}$  Pascals.<sup>52,53</sup> Ultra-high vacuum is conventionally defined to begin at pressures of  $10^{-7}$  and below. Extrapolating from the known data, we set a max temperature of 1000 K for UHV pressures, but later measurements at these pressures could decrease this value.

Now that both an acceleration distance and temperature have been calculated for all designs, we define a new and final composite figure of our sail design space analysis: Thermally Endurable Acceleration Minimum (TEAM). To find the TEAM values, we first eliminate all designs with  $T_{\max} > T_{\text{sublimation}}$  and find the minimum  $D$  design of those designs remaining. Minimizing TEAM is desirable, but we emphasize that this is not a sail *metric* per se; rather, it is a single summary value that can be easily reported to compare design approaches and sail datasets, as opposed to individual sails. For a given set of sail architectures, this final result is dependent on two quantities: the previously assumed maximum allowable sail temperature set by the UHV sublimation limit, and the assumed total absorptance of the sail.

While conventional photonic crystal slabs have desirable reflective properties from an accelerative standpoint, their thermal exitance is highly dependent on the both the amount

and spectral emissivity of their component materials. In the case of lightsails, a strong trade-off exists between having sufficient emissivity for heat dissipation and minimizing acceleration distance. For a given sail diameter, while acceleration distance is generally negatively impacted by mass increases, emissivity is generally rewarded by increasing the amount of emissive material per unit area. In analyzing our sail designs, we assume total sail absorption values ranging from  $10^{-4}\%$  to  $10^{-6}\%$  and show in Figure 3a the relationship between acceleration distance and operating temperature for three of these absorption values. Using the calculated maximum design temperature and acceleration distance  $D$  for each design, TEAM disqualifies all sails that lie above our UHV decomposition limit.

Using our framework, we demonstrate a TEAM value of 16.2 Gm, a 6.4 Gm accelerative penalty to prevent decomposition due to sublimation of Sulphur out of the  $\text{MoS}_2$  in the sail. Addition of a 1g mechanical backbone results in a TEAM value of 20.5 Gm. The improved temperature performance of the design that achieves the TEAM value is due to its smaller hole radius and thicker emissive  $\text{Si}_3\text{N}_4$  layers, and thus more material is present to enhance thermal performance. This can be seen in the comparison of the spectral hemispherical emissivity values of the TEAM design vs. the baseline acceleration distance-optimized design in Figure 3b. The TEAM design presents  $\sim 19\times$  higher peak emissivity value due to the presence of more  $\text{Si}_3\text{N}_4$  in the photonic crystal design. Alternatively, one can analyze the effect on the TEAM value as a function of overall sail absorption in the laser bandwidth. As can be seen in Figure 3c, when  $\alpha$  increases, TEAM will also increase, placing firm bounds on material absorption of the incident laser light given the need to achieve a certain acceleration distance.

Lower acceleration distances could be achieved if the sail's emissivity could be increased without sacrificing reflective behavior or adding mass. To this end, we propose a Mie resonant structure-based approach to emissivity gains that employs a multiscale design of thermal wavelength-scale Mie resonators patterned with laser wavelength-scale photonic crystal features, shown schematically in Figure 4a. The structure can be connected by a series of thin

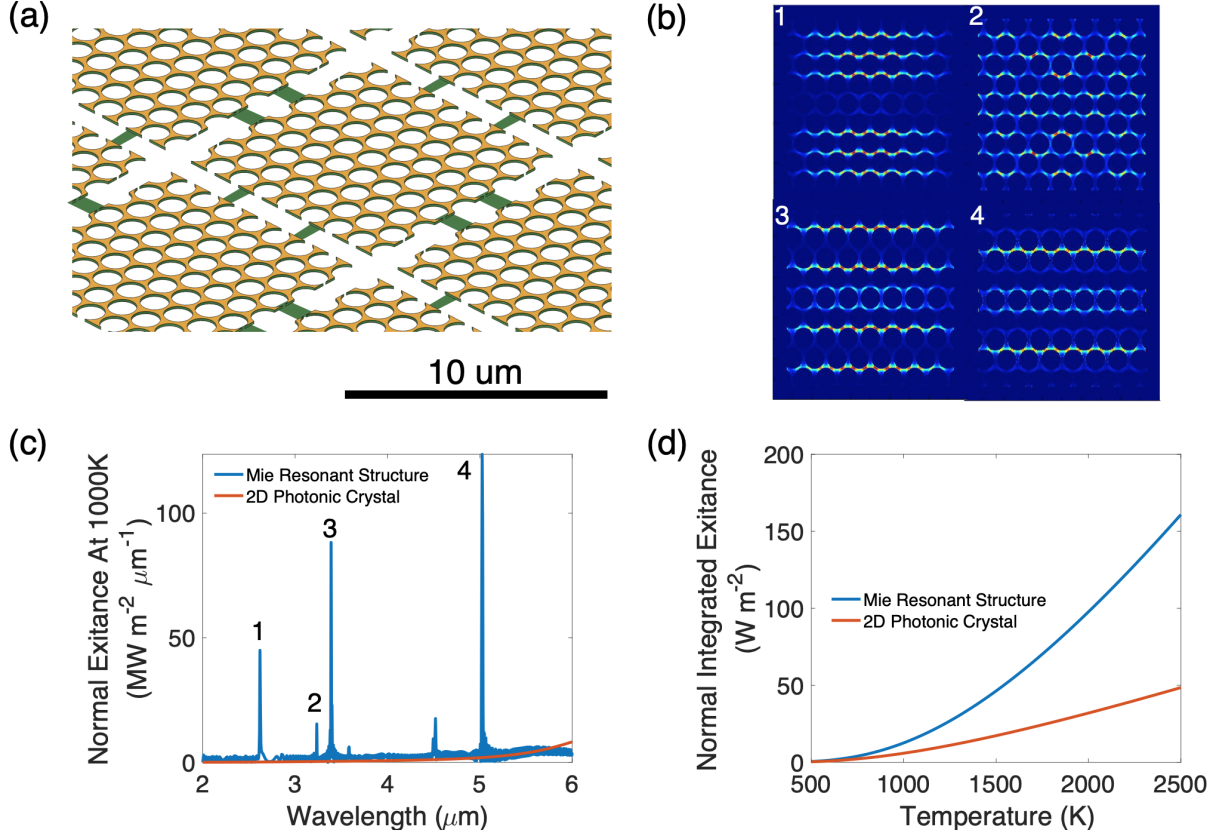


Figure 4: Mie resonant enhancement (a) schematic illustrating multiscale Mie resonator design. Green strips are scaffolds used as Mie resonator support structure. (b) Spatial absorption profile of Mie Resonances (c) 1000K normal exitance of Mie resonant structure vs conventional photonic crystal structure, demonstrating pathway for possible emissivity enhancement. Labelled wavelength peaks correspond to spatial profiles in (b). (d) demonstration of spectral integrated normal exitance enhancement as a function of temperature.

scaffolds while maintaining the presence of resonant modes. Four supported resonant mode spatial profiles, are shown in Figure 4b, corresponding to four modes in the 2 - 6 μm band shown in Figure 4c. We assert that this wavelength band is critical for sail heat management due to the blackbody peak position at temperatures from 500 - 1000K, as determined by Wien's law. Increases to sail emissivity in this band will more strongly reduce overall sail temperatures in comparison to emissivity increases at longer wavelengths. The enhancement in exitance at a given temperature is demonstrated in Figure 4d, showing that as much as 3 times the in-band normal exitance can be achieved for very high temperatures. This paves the way for future photonic strategies for emissivity engineering, and gives future sail

designers a new avenue for effective thermal management.

In conclusion, we have demonstrated holistically viable multilayer 2D photonic reflector designs for laser-driven lightsails that are able to accelerate to one fifth the speed of light over distances comparable to those of the best designs reported previously. We emphasize that our designs represent the entire sail structure and do not require additional backing material for emissivity enhancement, allowing for accurate modeling of payload-driven performance. To analyze this and other designs, we further proposed a new framework that judges sail designs according to both their acceleration distance and peak temperature. We then proposed the thermally durable acceleration minimum (TEAM) as a summary value to determine the fastest thermally-stable sail design of a design set. This value is easily reportable and will allow future designers to compare their design sets to others in the literature. Finally, we demonstrated how the use of Mie resonant feature patterning at thermal wavelength scales can act as a means of enhancing mid-infrared emissivity of sails while preserving their underlying acceleration distance characteristics. These results are an important step forward in designing and characterizing thermally viable lightsail designs for relativistic interstellar travel.

## 2 Methods

We performed reflective simulations using the  $S^4$  RCWA solver and Lumerical FDTD Solver. Simulations were performed over a Doppler-shifted wavelength band from 1.2-1.47  $\mu\text{m}$  for reflection. We performed absorptivity simulation in  $S^4$  from 1.55-14.05  $\mu\text{m}$ , using a reduced thickness scheme demonstrated in the supplemental information. Data was analyzed and merited using MATLAB R2020a and RStudio.

## Acknowledgement

This work was supported by the Breakthrough Initiatives, a division of the Breakthrough Prize Foundation. J.B. is supported by a National Science Foundation Graduate Research Fellowship under grants DGE-1650605 and DGE-2034835.

## References

- (1) Martin, A. R.; Bond, A. Nuclear pulse propulsion - A historical review of an advanced propulsion concept. 1979.
- (2) Beals, K. A.; Beaulieu, M.; Dembia, F. J.; Kerstiens, J.; Kramer, D. L.; West, J. R.; Zito, J. A. Project longshot: An unmanned probe to alpha centauri. **1988**,
- (3) Bond, A.; Group., P. D. S. *Project Daedalus : the final report on the BIS starship study*; British Interplanetary Society: London, England, 1978.
- (4) Long, K.; Obousy, R.; Hein, A. Project Icarus: Optimisation of nuclear fusion propulsion for interstellar missions. *Acta Astronautica* **2011**, *68*, 1820–1829.
- (5) Wagner, K. et al. Imaging low-mass planets within the habitable zone of  $\alpha$  Centauri. *Nature Communications* **2021**, *12*, 1–7.
- (6) Dumusque, X.; Pepe, F.; Lovis, C.; Ségransan, D.; Sahlmann, J.; Benz, W.; Bouchy, F.; Mayor, M.; Queloz, D.; Santos, N.; Udry, S. An Earth-mass planet orbiting  $\alpha$  Centauri B. *Nature* **2012**, *491*, 207–211.
- (7) Parkin, K. L. The Breakthrough Starshot system model. *Acta Astronautica* **2018**, *152*, 370–384.
- (8) Novotny, L.; Hecht, B. *Principles of Nano-Optics*, 2nd ed.; Cambridge University Press, 2012; p 448–473.

- (9) Garwin, R. L. Solar sailing—a practical method of propulsion within the solar system. 1958.
- (10) Drexler, K. E. High performance solar sails and related reflecting devices. Princeton University and American Institute of Aeronautics and Astronautics, Conference on Space Manufacturing Facilities, 4 th, Princeton University, Princeton, N. J. 1979.
- (11) Davoyan, A. R.; Munday, J. N.; Tabiryan, N.; Swartzlander, G. A.; Johnson, L. Photonic materials for interstellar solar sailing. *Optica* **2021**, *8*, 722.
- (12) Lingam, M.; Loeb, A. Propulsion of spacecrafts to relativistic speeds using natural astrophysical sources. *arXiv* **2020**, *894*, 36.
- (13) Wentzel-Long, M.; Landis, G. A. *AIAA Propulsion and Energy 2020 Forum*.
- (14) Forward, R. L. Roundtrip interstellar travel using laser-pushed lightsails. *Journal of Spacecraft and Rockets* **1984**, *21*, 187–195.
- (15) Kulkarni, N.; Lubin, P.; Zhang, Q. Relativistic spacecraft propelled by directed energy. *arXiv* **2017**, *155*, 155.
- (16) Redding, J. L. Interstellar vehicle propelled by terrestrial laser beam. *Nature* **1967**, *213*, 588–589.
- (17) Kipping, D. Relativistic light sails. *The Astronomical Journal* **2017**, *153*, 277.
- (18) Tsuda, Y.; Mori, O.; Funase, R.; Sawada, H.; Yamamoto, T.; Saiki, T.; Endo, T.; Kawaguchi, J. Flight status of IKAROS deep space solar sail demonstrator. *Acta Astronautica* **2011**, *69*, 833–840.
- (19) Atwater, H. A.; Davoyan, A. R.; Ilic, O.; Jariwala, D.; Sherrott, M. C.; Went, C. M.; Whitney, W. S.; Wong, J. Materials challenges for the Starshot lightsail. *Nature Materials* **2018**, *17*, 861–867.

- (20) Chou, S. Y.; Krauss, P. R.; Renstrom, P. J.; Chou, S. Y.; Krauss, P. R.; Renstrom, P. J. Imprint lithography with 25-nanometer resolution. *1996*, *272*, 85–87.
- (21) Chen, Y. Nanofabrication by electron beam lithography and its applications: A review. *Microelectronic Engineering* **2015**, *135*, 57–72.
- (22) Johnson, R. W.; Hultqvist, A.; Bent, S. F. A brief review of atomic layer deposition: From fundamentals to applications. *Materials Today* **2014**, *17*, 236–246.
- (23) Kolodziejski, L. A.; Fan, S.; Villeneuve, P.; Joannopoulos, J. D. Guided modes in photonic crystal slabs. *Physical Review B - Condensed Matter and Materials Physics* **1999**, *60*, 5751–5758.
- (24) Fan, S.; Joannopoulos, J. D. Analysis of guided resonances in photonic crystal slabs. *Physical Review B - Condensed Matter and Materials Physics* **2002**, *65*, 1–8.
- (25) Molesky, S.; Lin, Z.; Piggott, A. Y.; Jin, W.; Vucković, J.; Rodriguez, A. W. Inverse design in nanophotonics. *Nature Photonics* **2018**, *12*, 659–670.
- (26) Yu, N.; Capasso, F. Flat optics with designer metasurfaces. *Nature Materials* **2014**, *13*, 139–150.
- (27) Raman, A. P.; Anoma, M. A.; Zhu, L.; Rephaeli, E.; Fan, S. Passive radiative cooling below ambient air temperature under direct sunlight. *Nature* **2014**, *515*, 540.
- (28) Rephaeli, E.; Raman, A.; Fan, S. Ultrabroadband photonic structures to achieve high-performance daytime radiative cooling. *Nano Letters* **2013**, *13*, 1457–1461.
- (29) Hoang, T.; Lazarian, A.; Burkhart, B.; Loeb, A. The interaction of relativistic spacecrafts with the interstellar medium. *The Astrophysical Journal* **2017**, *837*, 5.
- (30) Hoang, T.; Loeb, A. Electromagnetic forces on a relativistic spacecraft in the interstellar medium. *arXiv* **2017**, *848*, 31.

- (31) Early, J. T.; London, R. A. Dust grain damage to interstellar laser-pushed lightsail. *Journal of Spacecraft and Rockets* **2000**, *37*, 526–531.
- (32) Manchester, Z.; Loeb, A. Stability of a light sail riding on a laser beam. *The Astrophysical Journal* **2017**, *837*, L20.
- (33) Ilic, O.; Went, C. M.; Atwater, H. A. Nanophotonic heterostructures for efficient propulsion and radiative cooling of relativistic light sails. *Nano Letters* **2018**, *18*, 5583–5589.
- (34) Ilic, O.; Atwater, H. A. Self-stabilizing photonic levitation and propulsion of nanostructured macroscopic objects. *Nature Photonics* **2019**, *13*, 289–295.
- (35) Salary, M. M.; Mosallaei, H. Photonic metasurfaces as relativistic light sails for doppler-broadened stable beam-riding and radiative cooling. *Laser and Photonics Reviews* **2020**, *1900311*, 1–19.
- (36) Salary, M. M.; Mosallaei, H. Inverse design of diffractive relativistic meta-sails via multi-objective optimization. *Advanced Theory and Simulations* **2021**, *2100047*, 1–16.
- (37) Jin, W.; Li, W.; Orenstein, M.; Fan, S. Inverse design of lightweight broadband reflector for relativistic lightsail propulsion. *ACS Photonics* **2020**, *7*, 2350–2355.
- (38) Gao, R.; Kim, Y.; Kim, L.; Kelzenberg, M. D.; Ilic, O.; Atwater, H. A. Self-stabilizing silicon nitride lightsails. *Conference Proceedings - Lasers and Electro-Optics Society Annual Meeting-LEOS* **2020**, *2020-May*, 4–5.
- (39) Boccara, A. C.; Jackson, W.; Amer, N. M.; Fournier, D. Sensitive photothermal deflection technique for measuring absorption in optically thin media. *Optics Letters* **1981**, *6*, 51.
- (40) Keevers, M. J.; Green, M. A. Absorption edge of silicon from solar cell spectral response measurements. *Applied Physics Letters* **1995**, *66*, 174–176.

- (41) Keevers, M. J.; Green, M. A. Absorption edge of silicon from solar cell spectral response measurements. *Applied Physics Letters* **1995**, *174*, 174.
- (42) Ermolaev, G. A.; Stebunov, Y. V.; Vyshnevyy, A. A.; Tatarkin, D. E.; Yakubovsky, D. I.; Novikov, S. M.; Baranov, D. G.; Shegai, T.; Nikitin, A. Y.; Arsenin, A. V.; Volkov, V. S. Broadband optical properties of monolayer and bulk MoS<sub>2</sub>. *npj 2D Materials and Applications* **2020**, *4*, 1–6.
- (43) Dumcenco, D.; Ovchinnikov, D.; Marinov, K.; Lazić, P.; Gibertini, M.; Marzari, N.; Sanchez, O. L.; Kung, Y.-C.; Krasnozhan, D.; Chen, M.-W.; Bertolazzi, S.; Gillet, P.; Fontcuberta i Morral, A.; Radenovic, A.; Kis, A. Large-area epitaxial monolayer MoS<sub>2</sub>. *ACS Nano* **2015**, *9*, 4611–4620.
- (44) Li, M.; Yao, J.; Wu, X.; Zhang, S.; Xing, B.; Niu, X.; Yan, X.; Yu, Y.; Liu, Y.; Wang, Y. P-type doping in large-area monolayer MoS<sub>2</sub> by chemical vapor deposition. *ACS Applied Materials & Interfaces* **2020**, *12*, 6276–6282.
- (45) Nie, C.; Yu, L.; Wei, X.; Shen, J.; Lu, W.; Chen, W.; Feng, S.; Shi, H. Ultrafast growth of large-area monolayer MoS<sub>2</sub> film via gold foil assistant CVD for a highly sensitive photodetector. *Nanotechnology* **2017**, *28*, 275203.
- (46) Myilswamy, K. V.; Krishnan, A.; Povinelli, M. L. Photonic crystal lightsail with non-linear reflectivity for increased stability. *Optics Express* **2020**, *28*, 8223.
- (47) Nishi, Y.; Doering, R. *Handbook of semiconductor manufacturing technology*; CRC press, 2000.
- (48) Haynes, W. M. *CRC handbook of chemistry and physics*; CRC press, 2014.
- (49) Kischkat, J.; Peters, S.; Gruska, B.; Semtsiv, M.; Chashnikova, M.; Klinkmüller, M.; Fedosenko, O.; MacHulik, S.; Aleksandrova, A.; Monastyrskyi, G.; Flores, Y.; Masselink, W. T. Mid-infrared optical properties of thin films of aluminum oxide, titanium

- dioxide, silicon dioxide, aluminum nitride, and silicon nitride. *Applied Optics* **2012**, *51*, 6789–6798.
- (50) Davami, K.; Zhao, L.; Lu, E.; Cortes, J.; Lin, C.; Lilley, D. E.; Purohit, P. K.; Bargatin, I. Ultralight shape-recovering plate mechanical metamaterials. *Nature Communications* **2015**, *6*, 1–7.
- (51) Campbell, M. F.; Brewer, J.; Jariwala, D.; Raman, A.; Bargatin, I. Relativistic light sails need to billow. 2021.
- (52) Cui, S.; Hu, B.; Ouyang, B.; Zhao, D. Thermodynamic assessment of the Mo-S system and its application in thermal decomposition of MoS<sub>2</sub>. *Thermochimica Acta* **2018**, *660*, 44–55.
- (53) Cannon, P. Melting point and sublimation of molybdenum disulphide. *Nature* **1959**, *183*, 1612–1613.